Construction of ZnO/Keggin Polyoxometalate Nano Heterojunction Catalyst For Efficient Removal of Rhodamine B in Aqueous Solution

Ruibo Guo
Qiqihar University
Liming Bai (blm68@163.com)
Qiqihar University https://orcid.org/0000-0002-5473-4734
Guohua Dong
Qiqihar University
Dongfeng Chai
Qiqihar University
Kun Lang
Qiqihar University
Zhonghua Mou
Qiqihar University
Ming Zhao
Qiqihar University

Research Article

Keywords: ZnO, Polyoxometalate, heterojunction, Photocatalysis

Posted Date: October 20th, 2021

DOI: https://doi.org/10.21203/rs.3.rs-973782/v1

Version of Record: A version of this preprint was published at Journal of Inorganic and Organometallic Polymers and Materials on March 3rd, 2022. See the published version at https://doi.org/10.1007/s10904-022-02251-x.

Abstract

In this paper, we synthesized two novel heterojunction nanocomposite catalysts ZnO/$Ag_4SiW_{12}O_{40}$ and ZnO/$Cs_3PW_{12}O_{40}$ by a simple dissolution-precipitation method. The structure and morphology of the samples were analyzed by XRD, TEM, FT-IR, Raman, UV diffuse reflection, XPS and N_2 adsorption desorption isotherm. Compared with pure ZnO, the composite catalyst formed with $Ag_4SiW_{12}O_{40}$(AgSiW) and $Cs_3PW_{12}O_{40}$(CsPW) can significantly improve the problem of fast recombination rate of photogenerated carriers in ZnO, and broaden the response range of ZnO to visible light. Rhodamine B (RhB) was used as a simulated pollutant to investigate the photocatalytic degradation performance of the composite catalyst. The experimental results show that the photocatalytic degradation activity of the prepared composite catalyst is much higher than that of pure ZnO, and the degradation performance of ZnO/$Ag_4SiW_{12}O_{40}$ is stronger. Finally, the possible photocatalytic mechanism of ZnO/$Ag_4SiW_{12}O_{40}$ and ZnO/$Cs_3PW_{12}O_{40}$ heterojunction nanocomposite catalysts was proposed by UV diffuse reflection, free radical capture experiment and Mott Schottky test.

1. Introduction

Due to the rapid development of industry, the environmental problems are becoming more and more serious. Water pollution is a difficult problem among many pollution problems, and the dye wastewater produced by the textile industry is an important source of water pollution. As pollutants, dyes have high molecular weight, complex structure and low biodegradability, while some dyes also have carcinogenicity and mutagenicity[1, 2]. Therefore, it is particularly important to find a method to deal with dye pollution. At present, photocatalytic technology is considered to be a clean, efficient and promising method to deal with dye pollution. It only needs photocatalyst and ubiquitous light to deal with pollutants. Compared with traditional methods, it will not cause secondary pollution and is cheap[3, 4].

Semiconductor materials, as a member of photocatalysts, are widely used because of their excellent properties[5]. Among many semiconductor materials, zinc oxide, as a wide gap material, has become one of the most studied and applied photocatalytic materials because of its stable physical and chemical properties, low cost and non-toxic[6, 7]. However, due to its wide band gap, it can only absorb ultraviolet light, which hinders the utilization of solar energy, and the recombination probability of photogenerated carriers is high, which affects its photocatalytic activity[8]. In order to improve the wide band gap of ZnO and the fast recombination rate of photogenerated carriers, predecessors have done a lot of work in this field, including controlling morphology, doping ions or metal elements and compounding with semiconductor materials[9, 10].

In order to improve the problems of ZnO in photocatalytic application, a method of compounding zinc oxide with heteropoly acid salt is proposed in this paper. Heteropoly acid is a catalyst with rich composition, structure and function. It has reversible redox properties and the ability to transfer and store electrons and protons[11, 12]. However, the application of heteropoly acids in the field of photocatalysis is in trouble because of their high solubility and difficult recovery. Based on the above problems, we

added $H_4SiW_{12}O_{40}$ and $H_3PW_{12}O_{40}$ into the synthesized zinc oxide system, introduced Ag and Cs metal cations respectively, and constructed $ZnO/Ag_4SiW_{12}O_{40}$ and $ZnO/Cs_3PW_{12}O_{40}$ heterojunction composite photocatalysts. The combination of heteropoly acid salt and zinc oxide not only improves the response range of ZnO to light, but also inhibits the rapid recombination of ZnO photogenerated carriers. The introduction of Ag and Cs metal cations also greatly improved the problem of high water solubility of heteropoly acids. It provides a new idea for the application of zinc oxide and heteropoly acid in the field of photocatalysis.

2. Materials And Methods

2.1 Chemicals

Silver nitrate, zinc chloride and sodium hydroxide were purchased from Tianjin Kaitong Chemical Reagent Co., Ltd. Caesium chloride were purchased from Shanghai Macklin Blochemical Co., Ltd. Silicotungstic acid and Phosphotungstic acid was products of Tianjin Guangfu Fine Chemical Research Institute. RhB was obtained from Shanghai McLean Biochemical Co., Ltd. Anhydrous ethanol was supplied by Tianjin Fuchen chemical reagent factory. All reagents are analytical grade and can be used without further purification. The secondary deionized water used was prepared in the laboratory.

2.2 Preparation of $ZnO/Ag_4SiW_{12}O_{40}$ and $ZnO/Cs_3PW_{12}O_{40}$

ZnO nanoparticles were synthesized by hydrothermal method. The specific synthesis process was as follows: 15 mL water solution with 1.36 g $ZnCl_2$ was added into 20 mL 1 mol/L NaOH solution and stirred evenly. Then, the mixture was transferred into a stainless steel autoclave lined with 50 mL polytetrafluoroethylene, reacted at 120℃ for 12 h, and naturally cooled to room temperature. After the precipitate was washed three times with deionized water and ethanol respectively, and then dried at 80℃, ZnO nanoparticles were obtained.

The synthesis process of nano-heterojunction photocatalyst was as follows: 0.5 g ZnO was evenly dispersed in 50 mL deionized water and the solution was ultrasonicated for 10 min. Add 0.6 mmol $H_4SiW_{12}O_{40}$ to the above solution and stir it with magnetic force for 2h, then 2.4 mmol $AgNO_3$ in the mixed solution and stir it at room temperature for 24h. The precipitate was obtained after the former mixed system was centrifuged. Then the fabricated nano-heterojunction $ZnO/Ag_4SiW_{12}O_{40}$ (ZnO/AgSiW) photocatalsyts were obtained after the precipitate was alternately washed three times with water and ethanol, and was dried overnight at 80℃. The preparation method of $ZnO/Cs_3PW_{12}O_{40}$(ZnO/CsPW) is similar, but the dosage of CsCl and $H_3PW_{12}O_{40}$ is changed (0.6 mmol CsCl and 0.2 mmol $H_3PW_{12}O_{40}$).

2.2 Characterization

The morphologies of the samples were characterized using transmission electron microscope (TEM) (Hitachi, H-7650, Japan). X-ray diffraction (XRD) analysis of samples was performed on X-ray diffractometer using Cu Kα radiation as X-ray source, operated at 60 kV and 80 mA (Bruker, AXS(D8),

German). X-ray photoelectron spectroscopy (XPS) was performed on electron spectrometer (VG, EscaLab 250Xi, Britain) with Al Kα X-ray radiation at 300 W. All binding energies were calibrated using C 1s peak at 284.8 eV. The Fourier Transform Infrared Spectrometer (FT-IR) spectrum was recorded employing Fourier transform infrared spectrophotometer (PE, America) at wavenumber range from 400 to 4000 cm^{-1} with KBr discs. Raman spectra of all samples were analyzed at room temperature by a Thermo Scientific DXR Smart Raman spectrometer (Thermo Electron Corporation, DXR2xi, America). The absorbance results were determined by the UV-vis dual-beam spectrophotometer (Persee, TU-1900, China) manufactured by Beijing General Electric Co., Ltd. The pore diameter of catalyst was determined by N_2 absorption-desorption isotherms (Quantachrome Nova Win2, American Kang Tai Company).

2.3 Photoelectrochemical measurements

Photocurrent measurements of conventional three electrode structure were carried out on CHI660E Electrochemical Workstation, including counter electrode, reference electrode and working electrode. The effective area of the working electrode prepared with the sample is about 1 cm^2. Platinum foil and Ag/AgCl electrode are used as counter electrode and reference electrode respectively. A 200 W (PLS-FX300HU, Nanjing chunyinjia Biotechnology Co., Ltd) xenon lamp was used as the light source. The electrolyte was 0.1 M Na_2SO_4 aqueous solution. In general, the preparation of working electrode is as follows: 40 mg of sample was suspended in 200 μL of prepared solution (1.8 mL of ethanol and 0.2 mL of naphthalene) and the slurry was obtained by ultrasonic treatment for 30 minutes. Then, 100 μL solution was evenly dropped onto 1×2 cm^2 FTO glass substrate. Finally, the working electrode was obtained by drying the prepared electrode at room temperature.

2.4 Photocatalytic measurements

(1) Photocatalytic activity evaluation

In this work, RhB was chosen as representative of organic pollutants. The process of photocatalytic experiment was as follows: in 50 mL quartz tube, 15 mg photocatalysts was dispersed in 50 mL RhB solution of 50 mg/L. The quartz tube was placed in a reactor with cooling water jacket. The mixture was stirred in dark for 30 min in to reach the adsorption saturation of RhB on nanophotocatalysts. Next, the reaction system was irradiated under 500 W xenon lamp. At 10 min intervals, 5 mL of the mixture was removed and centrifuged. The absorbance of supernatant was measured by UV spectrophotometer at 554 nm.

(2) Photocatalytic cycle performance test

After the single photocatalytic degradation reaction, the photocatalytic system was centrifuged and the solid catalyst was collected. Then, the catalyst was washed three times under ultrasound and dried at 60 ℃ for 12 h. The mass of the photocatalyst solid was weighed and supplemented to reach 15 mg with new catalyst that had not been subjected to the photocatalytic reaction. The rest of the experiment operations were same as the single reaction process.

(3) Scavenger experiment of photogenerated carriers

In order to identify the reactive species which play an important role in the photocatalytic degradation process, scavenger experiment of photogenerated carriers was carried out. For this purpose, p-benzoquinone, isopropanol and methanol were used as trapping agents for superoxide radical ($\cdot O_2^-$), hydroxyl radical (·OH) and hole (h^+) in the photocatalytic process. The rest of experiment process was same as the single photocatalytic reaction.

3. Results And Discussion

3.1 Crystal structure analysis

The phase structure of ZnO before and after compounding with AgSiW and CsPW was studied by XRD. The results are shown in Fig. 1. The characteristic peaks of AgSiW at 21.08, 23.58, 25.9, 28.0, 29.96, 31.86, 33.58, 35.3, 38.5, 41.46, 42.88, 44.3, 45.66, 46.98, 49.58, 54.4, 61.18 and 63.38° are consistent with the XRD spectra in the literature[13]. The characteristic peaks of CsPW appear at 10.54, 18.3, 23.7, 26.0, 30.22, 35.52, 38.72, 43.38, 47.18, 54.78 and 61.56°, which are consistent with those reported in the literature[14, 15]. The peaks of ZnO at 31.79, 34.43, 36.26, 47.52, 56.59, 62.85, 66.31, 67.94 and 69.08° are consistent with the standard card (PDF#65-3411), corresponding to the (100), (002), (101), (102), (110), (103), (200), (112) and (201) crystal planes of ZnO respectively. The characteristic peaks related to ZnO are shown in the spectra of ZnO/AgSiW and ZnO/CsPW composite catalysts, and the characteristic peaks of AgSiW (25.86, 28.04 and 30.08°) and CsPW (26.02°) can be observed in the spectra of ZnO/AgSiW and ZnO/CsPW, but the peak intensity is weak. It may be that the crystallinity of AgSiW and CsPW decreases or AgSiW are highly dispersed on the surface of ZnO during the formation of the complex, or it may be related to the low dosage of AgSiW and CsPW[16, 17].

3.2 Morphology analysis

The morphology of the prepared nanomaterials was determined by TEM. Fig. 2 shows TEM images of ZnO, AgSiW, CsPW, ZnO/AgSiW and ZnO/CsPW. It can be seen from the figure that the prepared samples are nano materials. In Fig. 2 (a), ZnO is a nano sheet with a size of about 100-400 nm and a thickness of about 30 nm. Fig. 2 (b) shows nano AgSiW. It can be seen from the image that AgSiW is massive, the size is about 200 nm, and nano dots with uniform size are distributed on the surface and edge. Fig. 2 (c) shows the TEM image of CsPW. It can be seen from the image that CsPW is a nanosphere with a diameter of 100-200 nm and has good dispersion. As can be seen from Fig. 2 (d), when ZnO and AgSiW form a composite, the morphology of AgSiW is changed, so that the massive AgSiW becomes dispersed and evenly distributed on the surface and edge of ZnO. It can also be seen from Fig. 2 (e) that there are ZnO and CsPW in the composite system, and they are closely combined. The results in Fig. 2 show that ZnO/AgSiW and ZnO/CsPW composite catalysts were successfully prepared.

3.3 FTIR analysis

In order to further determine the structure of the composite catalyst, the infrared spectra of the samples were analyzed. In the FT-IR spectrum, the characteristic bands of Keggin anion of AgSiW appear at 1020, 980, 926 and 783 cm^{-1}, corresponding to the stretching vibration of silver silicotungstate Si-O_a, W-O_d, W-O_b-W and W-O_c-W bonds respectively. The peak at 878 cm^{-1} may be due to the connection between counter ion and bridge oxygen W-O_b-W[13]. The peaks of CsPW at 1081, 989, 892 and 810 cm^{-1} are attributed to the stretching vibration of P-O_a, W=O_d, W-O_b-W and W-O_c-W, respectively[18]. The characteristic peaks of ZnO appear at 566 and 435 cm^{-1}, corresponding to the stretching vibration of zinc oxide Zn-O[19, 20]. It can be seen from the figure that in the spectra of ZnO/AgSiW and ZnO/CsPW, the characteristic peaks of AgSiW can be observed at 988, 912, 862 and 733 cm^{-1}, corresponding to the stretching vibration of Si-O_a, W-O_d, W-O_b-W and W-O_c-W bonds respectively, and the characteristic structures of CsPW can be observed at 1081, 988, 888 and 816 cm^{-1}, corresponding to the stretching vibration of P-O_a, W=O_d, W-O_b-W and W-O_c-W, respectively. Compared with ZnO/CsPW, AgSiW in ZnO/AgSiW composite catalyst shifted to a lower wave number, which may be related to the strong interaction between AgSiW and ZnO.

3.4 Raman spectra analysis

The Raman spectra of ZnO/AgSiW, ZnO/CsPW, ZnO, AgSiW and CsPW are shown in Fig. 4. The characteristic bands of Keggin anion of AgSiW appear at 983, 954, 883 and 559 cm^{-1}, corresponding to the asymmetric stretching mode of W=O_d, the symmetric stretching mode of W=O_d and W-O_b-W and the bending vibration of O-Si-O, respectively[21–23]. The peaks of CsPW at 1009 cm^{-1} and 994 cm^{-1} are attributed to the symmetrical and asymmetric stretching modes of W=O. The bands at 906 and 537 cm^{-1} are attributed to the asymmetric stretching mode of W-O-W and the bending vibration mode of O-P-O, respectively[24, 25]. The peaks at 336, 439 and 583 cm^{-1} belong to the vibration modes of 2E2 (M), E2 (high) and E1 (LO) of ZnO[26]. When ZnO and AgSiW are combined, a significantly enlarged band compared with AgSiW is observed at 897cm^{-1}, and there is an obvious displacement, indicating that there is a certain interaction between ZnO and AgSiW[27, 28]. However, no obvious characteristic peak of ZnO was observed in the spectrum, which may be due to the weak Raman intensity of ZnO after recombination. After ZnO and CsPW were compounded, the characteristic peaks belonging to ZnO and CsPW can be found in the spectrum, but the characteristic peak of CsPW is weaker than that of pure CsPW, which may be due to the low compounding amount of CsPW or the hydrogen bond interaction between the oxygen atom of Keggin anion and the hydroxyl group on the surface of ZnO[27].

3.5 Band gap analysis

The optical properties of ZnO/AgSiW, ZnO/CsPW, ZnO, AgSiW and CsPW were studied by measuring the UV diffuse reflectance spectra (DRS). The results are shown in Fig. 5. The illustrated part in the figure is calculated by formula (1). It can be estimated that the band gaps of ZnO/AgSiW, ZnO/CsPW, ZnO, AgSiW and CsPW are 2.53, 3.10, 3.15, 3.06 and 3.21eV respectively. It can be seen that the heterojunction system of ZnO with AgSiW and CsPW widens the absorption range of ZnO to light, and the effect of introducing

AgSiW is very obvious, which also makes ZnO/AgSiW make more full use of sunlight. This result may also be directly related to the stronger photocatalytic degradation of ZnO/AgSiW than ZnO/CsPW.

$(\alpha h\nu)^{1/n} = A(h\nu - Eg)$ (1)

Where, α , $h\nu$, E_g and A represent the absorption coeffificient, photon energy, band gap energy and a constant, respectively[16, 29].

3.6 XPS spectra of ZnO/AgSiW and ZnO/CsPW

Figure 6 shows the X-ray photoelectron spectroscopy (XPS) of the sample to further verify the elemental composition and chemical state of the synthetic sample. As shown in Fig. 6a, Zn 2p, Ag 3p, O 1s, W 4p, Ag 3d, C 1s, W 4d and W 4f signals are clearly displayed in the full scan measurement spectrum of ZnO/AgSiW. The low content of Zn 2p may be related to the uniform distribution of AgSiW on the surface of ZnO. The signals of Zn 2p, Cs 3d, O 1s, W 4p, C 1s, W 4d, Zn 3s, Zn 3p, W 4f and Zn 3d were clearly displayed in the full scanning measurement spectrum of ZnO/CsPW. The elemental composition of ZnO/AgSiW and ZnO/CsPW was determined by full spectrum scanning. Fig. 6b shows the XPS spectra of Zn 2p in ZnO/AgSiW, ZnO/CsPW and ZnO. Compared with the peaks of pure ZnO at 1021.63 eV (Zn $2p_{3/2}$) and 1044.63 eV (Zn $2p_{1/2}$), the Zn binding energy in ZnO/AgSiW and ZnO/CsPW samples shifted. Among them, the binding energy of Zn in ZnO/AgSiW samples shifts to the right, while the binding energy of Zn in ZnO/CsPW samples shifts to the left, indicating that there may be a certain interaction force between Zn and AgSiW and CsPW when ZnO forms a composite heterojunction system with AgSiW and CsPW. Figure 6 (c) and Figure 6 (d) show the XPS spectra of samples Ag 3d and Cs 3d respectively. The peaks at 366.88 and 372.88 eV are attributed to the $3d_{3/2}$ and $3d_{5/2}$ orbits of Ag (I), while the peaks at 724.78 and 738.68eV are attributed to the $3d_{3/2}$ and $3d_{5/2}$ orbits of Cs (I). Compared with the AgSiW and CsPW of monomers, the binding energy of Ag and Cs after composite has shifted[30]. Figure 6 (e) shows the W 4f XPS spectra of ZnO/AgSiW and ZnO/CsPW samples. In the spectrum of AgSiW, the peaks at 34.17 and 36.27 eV can be attributed to W (VI), and the peaks can be observed at 33.56 and 35.66 eV, indicating the presence of reduced W (V) in the complex. Compared with pure AgSiW, the binding energy of W shifted significantly to the right. In the spectrum of CsPW, the peaks at 36.22 and 38.36 eV can be attributed to W (VI), the peaks at 35.24 and 37.31 eV can be attributed to W (V), and the binding energy of W changes less than that of pure CsPW. Figure 6 (f) shows the O 1s XPS spectra of ZnO/AgSiW and ZnO/CsPW samples. The peaks at 528.84, 530.41 and 531.86 eV can be attributed to the lattice oxygen in ZnO, the lattice oxygen in Keggin structure (W-O-W) and Si-O bond in ZnO/AgSiW samples, respectively. The peaks at 531.06 and 532.39 eV can be attributed to the lattice oxygen and P-O bond in ZnO of ZnO/CsPW sample, respectively[31]. The above results show that when ZnO constructs a heterojunction system with AgSiW and CsPW, a strong interaction is formed, this result is also consistent with FT-IR and Raman spectra.

3.7 BET analysis

The surface area and pore structure of the samples were further analyzed by nitrogen adsorption desorption. As can be seen from Fig. 7 (a), ZnO and ZnO/AgSiW samples show type III isotherms with H3

hysteresis loops[32, 33], and ZnO/AgSiW samples show type IV isotherms with H3 hysteresis loops[34, 35], indicating that the samples have cracked mesoporous structure. The specific surface area of pure ZnO is 13.043 m^2/g. When the heterojunction system was constructed with ZnO/CsPW and ZnO/AgSiW, the specific surface areas of the heterojunction catalysts were 13.032 and 8.191 m^2/g, respectively. It can be seen from Fig. 7 (b) that the introduction of CsPW and AgSiW has a certain impact on the pore size of ZnO, and AgSiW has a significant impact on the specific surface area of the heterojunction system. The possible reason is that AgSiW is evenly dispersed on the surface of ZnO and strongly coupled with ZnO[36], which is consistent with the TEM results.

3.8 Photocatalytic activity

The photocatalytic activities of ZnO/AgSiW and ZnO/CsPW samples were tested with RhB as the target pollutant. Under the irradiation of simulated sunlight, the removal effect of the catalyst on dyes was evaluated under the conditions of catalyst dosage of 15 mg and dye concentration of 50 mL. According to Fig. 8 (a), the degradation rates of RhB by ZnO/AgSiW, ZnO/CsPW and ZnO are 92.3%, 72.7% and 17.2% respectively. The results show that the catalytic performance of the prepared ZnO/AgSiW and ZnO/CsPW composite catalysts is greatly improved compared with pure ZnO. Although pure AgSiW and CsPW have strong adsorption properties, they hardly have catalytic properties. However, when combined with ZnO, the composite system showed high catalytic activity, which may be because AgSiW and CsPW constructed a heterojunction system with ZnO, which improved the problem of fast recombination rate of ZnO photogenerated carriers and widened the absorption range of ZnO to light. As can be seen from Fig. 8 (b), $\ln(C_0/C_t)$ has a good linear relationship with time, indicating that the photocatalytic degradation of RhB by ZnO, ZnO/AgSiW and ZnO/CsPW conforms to the pseudo first-order kinetic model:

$$\mathrm{L}\left(\frac{C_0}{C_t}\right) = k_{app}t \quad (2)$$

where k_{app} is the apparent rate constant (min^{-1}), t is the irradiation time (min), C_o and C_t are the absorbance at t = 0 min and t = ∞[12].

The calculated k_{app} values of ZnO/AgSiW, ZnO/CsPW and ZnO are 0.0403, 0.0203 and 0.0028 min^{-1} respectively, and the reaction rate constants of ZnO/AgSiW and ZnO/CsPW are 14.4 and 7.3 times that of ZnO, respectively. The results show that the two composite catalysts have stronger catalytic activity than pure ZnO.

3.9 Recyclability of photocatalysts

In addition to the efficiency of photocatalysts, the stability and recoverability of photocatalysts are also important indicators to evaluate whether they can be applied to practice. In order to explore the stability and recoverability of photocatalyst, it was studied by cyclic experiment. As shown in Fig. 9, under simulated sunlight, the removal rates of RhB by ZnO/AgSiW and ZnO/CsPW for the first time are 91.3% and 73.7% respectively. After the two catalysts are recycled for 3 times, the removal rates of RhB are

84.8% and 65.3% respectively. They still have high photocatalytic activity, which proves the stability and recoverability of the complex as a catalyst.

3.10 Reaction mechanism

To confirm the effective separation of photogenerated carriers, the transient photocurrent response and electrochemical impedance were measured. Fig. 10 (a) shows the transient photocurrent response of ZnO, ZnO/AgSiW and ZnO/CsPW under visible light irradiation. As can be seen from the figure, when the light is switched in three cycles, the generated photocurrent is stable and repeatable. Under visible light irradiation, it can be clearly seen that the photocurrent density of ZnO/AgSiW and ZnO/CsPW is higher than that of ZnO, and the higher the photocurrent density, the lower the efficiency of photoinduced charge recombination[37, 38], which means that the charge separation of the two heterojunction heterojunction catalysts has been improved and the charge separation rate of the composite catalysts has been greatly improved. The Nyquist curve is shown in Fig. 10 (b). Generally, the arc radius on the EIS Nyquist diagram corresponds to the charge transfer resistance (Rct), while the small arc radius represents the low charge transfer resistance[39, 40]. Obviously, ZnO/AgSiW and ZnO/CsPW composite catalysts have lower charge transfer resistance than ZnO, which means that the formed composite system can effectively improve the charge transfer between interfaces. This result is consistent with the photocurrent response, which shows that the composite system formed by ZnO, AgSiW and CsPW can significantly improve the separation efficiency of photogenerated carriers, improve the charge transfer between interfaces, and then improve the photocatalytic degradation performance.

3.11 Free radical capture experiment

Figure 11 is a free radical capture experiment to determine the active substances that play a major role in the photocatalytic process. P-benzoquinone, isopropanol and methanol were used as capture agents for superoxide anion radical, hydroxyl radical and hole. It can be seen from the left half of Figure 11 that the addition of p-benzoquinone has the greatest impact on the photocatalytic activity of ZnO/AgSiW composite catalyst, followed by methanol, indicating that superoxide anion free radicals and holes play the main catalytic role in the photocatalytic process, while the addition of isopropanol has relatively little impact on the photocatalytic activity, indicating that holes also hinder the degradation reaction, But not the main active substance. It can be seen from the right half of Figure 11 that the addition of isopropanol and methanol has the greatest impact on the photocatalytic activity of ZnO/CsPW composite catalyst, indicating that hydroxyl radical and hole are the main active substances in the photocatalytic reaction process, and also plays a certain inhibitory role after the addition of p-benzoquinone, indicating that superoxide anion radical is also produced in the photocatalytic process.

On this basis, the possible mechanisms of photocatalytic degradation of RhB by ZnO/AgSiW and ZnO/CsPW were proposed. The band gaps of ZnO, AgSiW and CsPW can be estimated to be 3.15, 3.06 and 3.21 eV respectively according to the UV Vis diffuse reflectance spectra. The measured potential and Ag/AgCl were converted to the normal hydrogen electrode (NHE) scale by equation (3) [41]:

$E_{NHE}=E_{Ag/AgCl}+0.197$ (4)

Therefore, the CB of ZnO, AgSiW and CsPW can be estimated by Mott-Schottky, which are -0.34, 0.76 and -0.01 eV respectively. The VB of ZnO, AgSiW and C_SPW can be calculated according to formula (4)[42], which are 2.81, 3.29 and 3.09 eV respectively.

$E_{VB} = E_{CB}+E_g$ (4)

According to the estimated conduction band and valence band positions, the possible mechanism diagrams of photocatalytic degradation of RhB by ZnO/AgSiW and ZnO/CsPW were constructed. As shown in Fig. 13, it is assumed that ZnO and AgSiW form a Z-scheme heterojunction. Under the irradiation of simulated sunlight, electrons are excited from VB of ZnO to CB, and photogenerated holes are left in VB. Because the CB of ZnO is more negative than $O_2/\cdot O_2^-$ potential (-0.046V vs. NHE)[41, 43], electrons on CB of ZnO can form $\cdot O_2^-$ with oxygen, and the formed $\cdot O_2^-$ can directly react with RhB molecule in water.

In AgSiW, the electrons are transferred from VB to CB and combined with the holes on VB of ZnO. This electron transfer can reduce the opportunity of electron hole recombination formed in ZnO and improve the photocatalytic activity. Because the VB (+ 2.81V vs. NHE) of ZnO is more positive than that of $OH^-/\cdot OH$ and $H_2O/\cdot OH$ (+ 1.99 V vs. NHE and + 2.27 V vs. NHE), the holes left on VB of AgSiW will be combined with H_2O and converted into ·OH.

According to the capture experiment, only a small part will react with H_2O and convert into ·OH, and the remaining holes will directly participate in the degradation of RhB. The other inference is inconsistent with the free radical capture experiment, because when the electrons on CB of ZnO are transferred to the CB of AgSiW and accumulated, the CB (+0.76V vs. NHE) of AgSiW is positive than the $O_2/\cdot O_2^-$ potential (-0.046V vs. NHE). AgSiW is a deep electron trap, which makes it difficult for electrons to jump out of AgSiW, so that the conversion from O_2 to $\cdot O_2^-$ is blocked[44].

According to the free radical capture experiment, holes and hydroxyl radicals play a major role in the photocatalytic process, and superoxide anion radicals also play a certain inhibitory role. As shown in Fig. 14, assuming that a Z-scheme heterojunction is formed between the samples, when the electrons on VB of ZnO and CsPW are excited and migrated to CB under the irradiation of sunlight, holes are left on VB, and the electrons on CB of CsPW migrate to the VB of ZnO. Because the potential of ZnO (-0.34 V vs. NHE) is more negative than that of $O_2/\cdot O_2^-$ (-0.046 V vs. NHE), O_2 can combine with the electrons on CB of ZnO to form $\cdot O_2^-$, while the potential of VB of C_SPW (+ 2.81v vs. NHE) is positive than that of $OH^-/\cdot OH$ and $H_2O/\cdot OH$(+ 1.99 V vs. NHE and + 2.27 V vs. NHE). Therefore, some holes on VB of C_SPW can react with water to form hydroxyl radicals, and the remaining holes directly play the role of oxidative degradation of RhB. If the type II heterojunction is formed, when the electrons on the CB of ZnO are transferred to the CB of C_SPW, because the potential of the CB of C_SPW is positive than the potential of

$O_2/\cdot O_2^-$ (-0.046 V vs. NHE), as a shallow electron trap, the electrons are not easy to react with O_2 to generate superoxide anion radicals, which is inconsistent with the experimental results of radical capture. Therefore, it is inferred that a Z-scheme heterojunction is formed between ZnO and C_SPW.

4. Conclusions

In conclusion, ZnO/AgSiW and ZnO/CsPW nano heterojunction composite catalysts were successfully synthesized by a simple dissolution-precipitation method. Taking RhB as the target pollutant, the photocatalytic activities of ZnO/AgSiW and ZnO/CsPW were tested under simulated sunlight. The experimental results show that the first-order kinetics of RhB degradation by ZnO/AgSiW and ZnO/CsPW, and k_{app}(ZnO/AgSiW) > k_{app}(ZnO/CsPW) > k_{app}(ZnO), compared with pure ZnO, the reaction rate constants of ZnO/AgSiW and ZnO/CsPW are 14.4 and 7.3 times that of ZnO, respectively. The results show that the two composite catalysts have stronger catalytic activity than pure ZnO. According to the cyclic experiment, the two catalysts still have high catalytic activity after three cycles. Therefore, the preparation of ZnO/AgSiW and ZnO/CsPW nano heterojunction composite catalysts provides a possibility for the construction of heteropoly acid salt and ZnO nano heterojunction system.

Declarations

Acknowledgements

This work was supported by the Innovation Project of Graduate Education of Qiqihar University (Grant No. YJSCX2020034) and Heilongjiang Industrial Hemp Processing Technology Innovation Center.

No conflict of interest exits in the submission of this manuscript, and the manuscript is approved by all authors for publication. I would like to declare on behalf of my co-authors that the work described was original research that has not been published previously, and not under consideration for publication elsewhere in whole or in part. All the authors listed have approved the manuscript that is enclosed.

References

1. T.D. Guidolin, N.M. Possolli, M.B. Polla, T.B. Wermuth, T.F.D. Oliveira, S. Eller, O.R.K. Montedo, S. Arcaro, M.A.P. Cechinel, *Photocatalytic pathway on the degradation of methylene blue from aqueous solutions using magnetite nanoparticles* (JOURNAL OF CLEANER PRODUCTION, 2021), p. 318
2. S. Kim, J. Yeo, W. Choi, *Simultaneous conversion of dye and hexavalent chromium in visible light-illuminated aqueous solution of polyoxometalate as an electron transfer catalyst*, 84 (APPLIED CATALYSIS B-ENVIRONMENTAL, 2008), pp. 148–155
3. T.T. Qiang, L. Chen, Y.J. Xia, X.T. Qin, *Dual modified MoS2/SnS2 photocatalyst with Z-scheme heterojunction and vacancies defects to achieve a superior performance in Cr (VI) reduction and dyes degradation* (JOURNAL OF CLEANER PRODUCTION, 2021), p. 291

4. J.J. He, H.Q. Sun, S. Indrawirawan, X.G. Duan, M.O. Tade, S.B. Wang, *Novel polyoxometalate@g-C3N4 hybrid photocatalysts for degradation of dyes and phenolics*, 456 (JOURNAL OF COLLOID AND INTERFACE SCIENCE, 2015), pp. 15–21
5. Y. Zhang, M.Y. Xiong, A.R. Sun, Z. Shi, B. Zhu, D.K. Macharia, F. Li, Z.G. Chen, J.S. Liu, L.S. Zhang, *MIL-101(Fe) nanodot-induced improvement of adsorption and photocatalytic activity of carbon fiberiTiO(2)-based weavable photocatalyst for removing pharmaceutical pollutants* (JOURNAL OF CLEANER PRODUCTION, 2021), p. 290
6. C. Shi, L.L. Zhang, H.Y. Bian, Z.J. Shi, J.X. Ma, Z.G. Wang, *Construction of Ag-ZnO/cellulose nanocomposites via tunable cellulose size for improving photocatalytic performance* (JOURNAL OF CLEANER PRODUCTION, 2021), p. 288
7. S.S. Yi, J.B. Cui, S. Li, L.J. Zhang, D.J. Wang, Y.H. Lin, Enhanced visible-light photocatalytic activity of Fe/ZnO for rhodamine B degradation and its photogenerated charge transfer properties. Appl. Surf. Sci. **319**, 230–236 (2014)
8. S. Wu, Z.W. Chen, T. Wang, X.H. Ji, A facile approach for the fabrication of Au/ZnO-hollow-sphere-monolayer thin films and their photocatalytic properties. Appl. Surf. Sci. **412**, 69–76 (2017)
9. R.E. Adam, H. Alnoor, G. Pozina, X.J. Liu, M. Willander, O. Nur, Synthesis of Mg-doped ZnO NPs via a chemical low-temperature method and investigation of the efficient photocatalytic activity for the degradation of dyes under solar light, SOLID STATE SCIENCES, 99 (2020)
10. H. Wang, C.C. Wang, Q.F. Chen, B.S. Ren, R.F. Guan, X.F. Cao, X.P. Yang, R. Duan, Interface-defect-mediated photocatalysis of mesocrystalline ZnO assembly synthesized in-situ via a template-free hydrothermal approach. Appl. Surf. Sci. **412**, 517–528 (2017)
11. R.X. Wang, L.F. Dang, Y.F. Liu, W.Z. Jiao, Preparation, characterization and photocatalytic activity of Dawson type phosphotungstate/graphene oxide composites. ADVANCED POWDER TECHNOLOGY **30**, 1400–1408 (2019)
12. S. Sampurnam, S. Muthamizh, T. Dhanasekaran, D. Latha, A. Padmanaban, P. Selvam, A. Stephen, V. Narayanan, *Synthesis and characterization of Keggin-type polyoxometalate/zirconia nanocomposites-Comparison of its photocatalytic activity towards various organic pollutants*, 370 (JOURNAL OF PHOTOCHEMISTRY AND PHOTOBIOLOGY A-CHEMISTRY, 2019), pp. 26–40
13. W.H. Zhou, M.H. Cao, S.Y. Su, N. Li, X.Y. Zhao, J.Q. Wang, X.H. Li, C.W. Hu, *A newly-designed polyoxometalate-based plasmonic visible-light catalyst for the photodegradation of methyl blue*, 371 (JOURNAL OF MOLECULAR CATALYSIS A-CHEMICAL, 2013), pp. 70–76
14. L. Li, C.J. Zou, L. Zhou, L. Lin, Cucurbituril-protected $Cs_{2.5}H_{0.5}PW_{12}O_{40}$ for optimized biodiesel production from waste cooking oil. RENEWABLE ENERGY **107**, 14–22 (2017)
15. M.A. Alotaibi, M.A. Bakht, A.I. Alharthi, M.H. Geesi, M.B. Alshammari, Y. Riadi, *Facile preparation of cesium salt of tungstophosphoric acid for catalytic synthesis of one-pot two-component 1,3,4-oxadiazole derivatives in water: A doubly green approach* (SUSTAINABLE CHEMISTRY AND PHARMACY, 2020), p. 17

16. Q. Cen, Q.Y. Gao, C.L. Zhang, Y.Q. Liu, Q. Wang, Q. Wang, *Photocatalytic reduction of Cr(VI) by iron tungstosilicate under visible light*, 562 (JOURNAL OF COLLOID AND INTERFACE SCIENCE, 2020), pp. 12–20
17. J.A. Rengifo-Herrera, M. Blanco, J. Wist, P. Florian, L.R. Pizzio, *TiO_2 modified with polyoxotungstates should induce visible-light absorption and high photocatalytic activity through the formation of surface complexes*, 189 (APPLIED CATALYSIS B-ENVIRONMENTAL, 2016), pp. 99–109
18. Y.G. Yu, Z.H. Lu, H. Wei, X.F. Cao, K.B. Li, *Electrostatic Self-assembly Aided Synthesis of $CdS/Cs_3PW_{12}O_{40}$ Hybrids for Photocatalytic Reduction of Cr(VI)* (WATER AIR AND SOIL POLLUTION, 2020), p. 231
19. M. Suresh, A. Sivasamy, *Fabrication of graphene nanosheets decorated by nitrogen-doped ZnO nanoparticles with enhanced visible photocatalytic activity for the degradation of Methylene Blue dye* (JOURNAL OF MOLECULAR LIQUIDS, 2020), p. 317
20. S. Bousalem, F.Z. Zeggai, H. Baltach, A. Benyoucef, Physical and electrochemical investigations on hybrid materials synthesized by polyaniline with various amounts of ZnO nanoparticle, CHEMICAL PHYSICS LETTERS, 741 (2020)
21. N. Songsiri, G.L. Rempel, P. Prasassarakich, Liquid-phase synthesis of isoprene from MTBE and formalin using cesium salts of silicotungstic acid. MOLECULAR CATALYSIS **439**, 41–49 (2017)
22. G. Raveendra, A. Rajasekhar, M. Srinivas, P.S.S. Prasad, N. Lingaiah, *Selective etherification of hydroxymethylfurfural to biofuel additives over Cs containing silicotungstic acid catalysts*, 520 (APPLIED CATALYSIS A-GENERAL, 2016), pp. 105–113
23. S.H. Zhu, X.Q. Gao, Y.L. Zhu, Y.F. Zhu, X.M. Xiang, C.X. Hu, Y.W. Li, *Alkaline metals modified Pt-$H_4SiW_{12}O_{40}/ZrO_2$ catalysts for the selective hydrogenolysis of glycerol to 1,3-propanediol*, 140 (APPLIED CATALYSIS B-ENVIRONMENTAL, 2013), pp. 60–67
24. I. Holclajtner-Antunovic, D. Bajuk-Bogdanovic, A. Popa, B.N. Vasiljevic, J. Krstic, S. Mentus, S. Uskokovic-Markovic, Structural, morphological and catalytic characterization of neutral Ag salt of 12-tungstophosphoric acid: Influence of preparation conditions. Appl. Surf. Sci. **328**, 466–474 (2015)
25. R. Liu, T.F. Wang, C. Liu, Y. Jin, Highly selective and stable $CsPW/Nb_2O_5$ catalysts for dehydration of glycerol to acrolein. CHINESE JOURNAL OF CATALYSIS **34**, 2174–2182 (2013)
26. N. Srinivasan, M. Anbuchezhiyan, S. Harish, S. Ponnusamy, Hydrothermal synthesis of C doped ZnO nanoparticles coupled with $BiVO_4$ and their photocatalytic performance under the visible light irradiation. Appl. Surf. Sci. **494**, 771–782 (2019)
27. G. Marci, E. Garcia-Lopez, V. Vaiano, G. Sarno, D. Sannino, L. Palmisano, Keggin heteropolyacids supported on TiO_2 used in gas-solid (photo)catalytic propene hydration and in liquid-solid photocatalytic glycerol dehydration. CATALYSIS TODAY **281**, 60–70 (2017)
28. M. Lafuente, I. Pellejero, A. Clemente, M.A. Urbiztondo, R. Mallada, S. Reinoso, M.P. Pina, L.M. Gandia, *Situ Synthesis of SERS-Active Au@POM Nanostructures in a Microfluidic Device for Real-Time*

Detection of Water Pollutants, 12 (ACS APPLIED MATERIALS & INTERFACES, 2020), pp. 36458–36467

29. N. Tahmasebi, S. Mirzavand, A. Hakimyfard, S. Barzegar, The excellent photocatalytic activity of novel $Cs_3PW_{12}O_{40}/WO_3$ composite toward the degradation of rhodamine B. ADVANCED POWDER TECHNOLOGY **30**, 257–265 (2019)
30. Y.L. Zhang, L.L. Hu, S.Y. Zhao, N.Y. Liu, L. Bai, J. Liu, H. Huang, Y. Liu, Z.H. Kang, $Ag_3PW_{12}O_{40}/C_3N_4$ nanocomposites as an efficient photocatalyst for hydrocarbon selective oxidation. RSC ADVANCES **6**, 60394–60399 (2016)
31. W. Li, T.T. Li, G.T. Li, L.B. An, F. Li, Z.M. Zhang, Electrospun H4SiW12O40/cellulose acetate composite nanofibrous membrane for photocatalytic degradation of tetracycline and methyl orange with different mechanism. CARBOHYDRATE POLYMERS **168**, 153–162 (2017)
32. R.W. Yang, J.H. Cai, K.L. Lv, X.F. Wu, W.G. Wang, Z.H. Xu, M. Li, Q. Li, W.Q. Xu, *Fabrication of TiO2 hollow microspheres assembly from nanosheets (TiO2-HMSs-NSs) with enhanced photoelectric conversion efficiency in DSSCs and photocatalytic activity*, 210 (APPLIED CATALYSIS B-ENVIRONMENTAL, 2017), pp. 184–193
33. C. Amirthavalli, A. Manikandan, A.A.M. Prince, Effect of zinc precursor ratio on morphology and luminescent properties of ZnO nanoparticles synthesized in CTAB medium. CERAMICS INTERNATIONAL **44**, 15290–15297 (2018)
34. J.M. Fang, J.D. Xu, J.H. Chen, X.Y. Huang, X. Wang, *Enhanced photocatalytic activity of molecular imprinted nano alpha-Fe_2O_3 by hydrothermal synthesis using methylene blue as structure-directing agent*, 508 (COLLOIDS AND SURFACES A-PHYSICOCHEMICAL AND ENGINEERING ASPECTS, 2016), pp. 124–134
35. J. Lu, Y. Wang, J.F. Huang, L.Y. Cao, J.Y. Li, G.J. Hai, Z. Bai, *One-step synthesis of g-C_3N_4 hierarchical porous structure nanosheets with dramatic ultraviolet light photocatalytic activity*, 214 (MATERIALS SCIENCE AND ENGINEERING B-ADVANCED FUNCTIONAL SOLID-STATE MATERIALS, 2016), pp. 19–25
36. C.H. Deng, H.M. Hu, H. Yu, M. Wang, M.Y. Ci, L.L. Wang, S.N. Zhu, Y.P. Wu, H.R. Le, 1D hierarchical CdS NPs/NiO NFs heterostructures with enhanced photocatalytic activity under visible light irradiation. ADVANCED POWDER TECHNOLOGY **31**, 3158–3167 (2020)
37. Q. Wang, E.Q. Liu, C.L. Zhang, S.W. Huang, Y.Q. Cong, Y. Zhang, *Synthesis of $Cs_3PMo_{12}O_{40}/Bi_2O_3$ composite with highly enhanced photocatalytic activity under visible-light irradiation*, 516 (JOURNAL OF COLLOID AND INTERFACE SCIENCE, 2018), pp. 304–311
38. X.F. Wu, X.F. Zhang, S. Zhao, Y. Gong, R. Djellabi, S. Lin, X. Zhao, *Highly-efficient photocatalytic hydrogen peroxide production over polyoxometalates covalently immobilized onto titanium dioxide* (APPLIED CATALYSIS A-GENERAL, 2020), p. 591
39. S.T. Li, P.F. Wang, R.D. Wang, Y.F. Liu, R.S. Jing, Z. Li, Z.L. Meng, Y.Y. Liu, Q. Zhang, One-step co-precipitation method to construct black phosphorus nanosheets/ZnO nanohybrid for enhanced visible light photocatalytic activity, Appl. Surf. Sci., 497 (2019)

40. H.W. Guo, J. Ding, S.P. Wan, Y.N. Wang, Q. Zhong, Highly efficient CH_3OH production over $Zn_{0.2}Cd_{0.8}S$ decorated g-C_3N_4 heterostructures for the photoreduction of CO_2, Appl. Surf. Sci., 528 (2020)
41. H.F. Shi, G. Yan, Y. Zhang, H.Q. Tan, W.Z. Zhou, Y.Y. Ma, Y.G. Li, W.L. Chen, E.B. Wang, *Ag/$Ag_xH_{3-x}PMo_{12}O_{40}$ Nanowires with Enhanced Visible-Light-Driven Photocatalytic Performance*, 9 (ACS APPLIED MATERIALS & INTERFACES, 2017), pp. 422–430
42. M. Mousavi, A. Habibi-Yangjeh, M. Abitorabi, *Fabrication of novel magnetically separable nanocomposites using graphitic carbon nitride, silver phosphate and silver chloride and their applications in photocatalytic removal of different pollutants using visible-light irradiation*, 480 (JOURNAL OF COLLOID AND INTERFACE SCIENCE, 2016), pp. 218–231
43. H.G. Yu, R. Liu, X.F. Wang, P. Wang, J.G. Yu, *Enhanced visible-light photocatalytic activity of Bi_2WO_6 nanoparticles by Ag2O cocatalyst*, 111 (APPLIED CATALYSIS B-ENVIRONMENTAL, 2012), pp. 326–333
44. J.H. Duan, M.Y. Liu, Y. Guo, W.W. Wang, Z.S. Zhang, C.J. Li, *High photocatalytic activity of 2D sheet structure ZnO/Bi_2WO_6 Z-scheme heterojunction under simulated sunlight* (JOURNAL OF PHYSICS D-APPLIED PHYSICS, 2020), p. 53

Figures

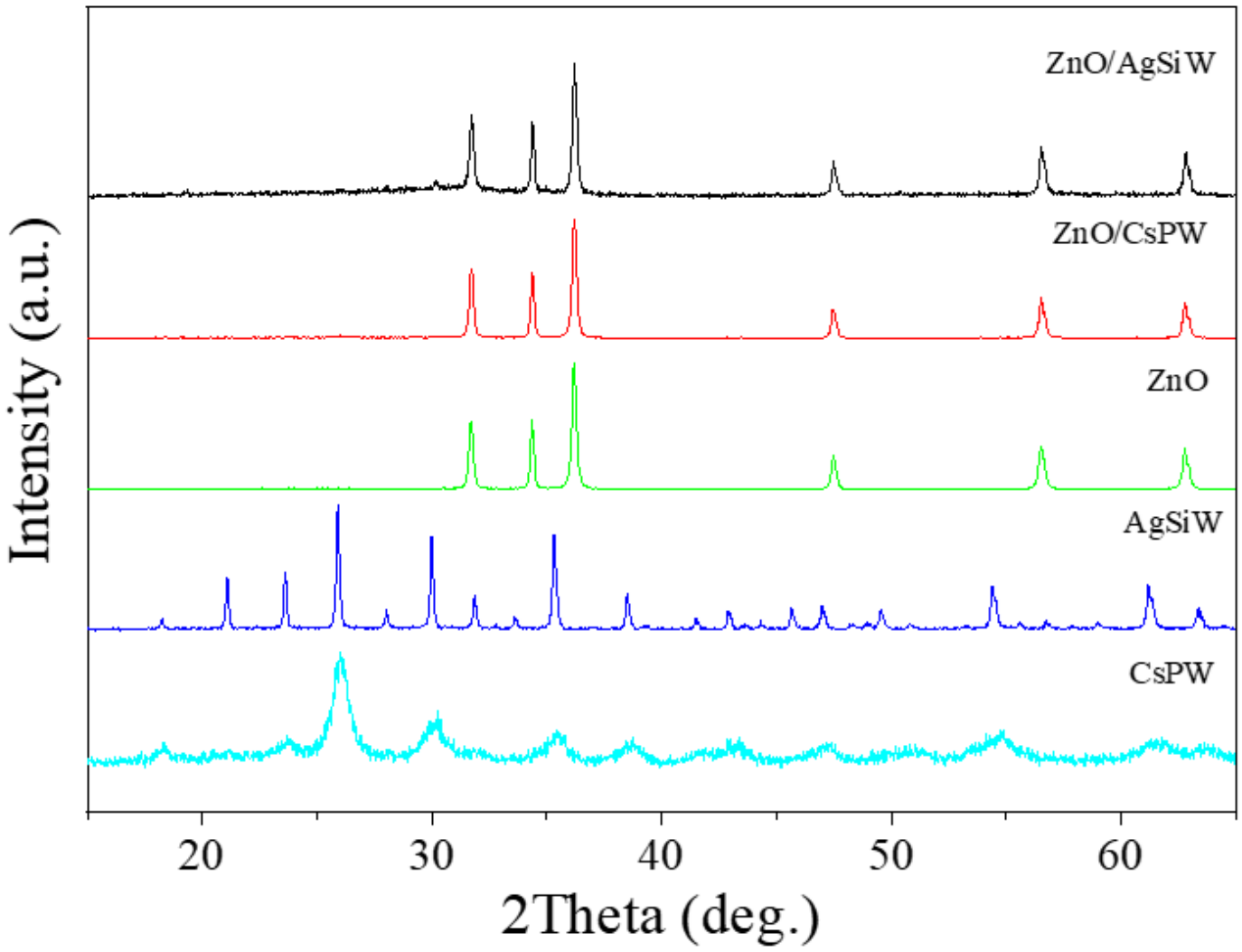

Figure 1

XRD patterns of ZnO/AgSiW, ZnO/CsPW, ZnO, AgSiW and CsPW

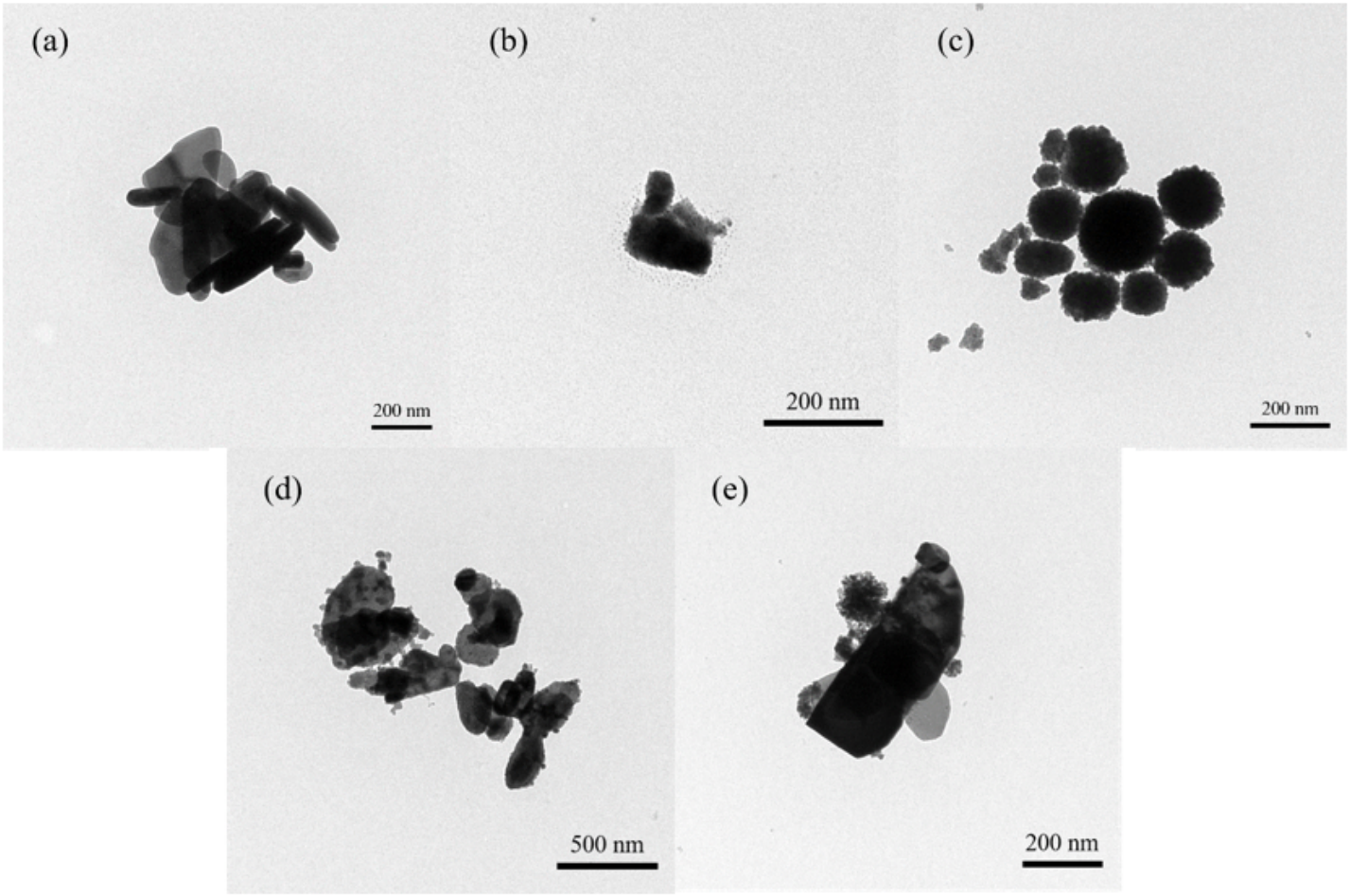

Figure 2

TEM images of ZnO (a), AgSiW (b), CsPW (c), ZnO/AgSiW (d) and ZnO/CsPW (e)

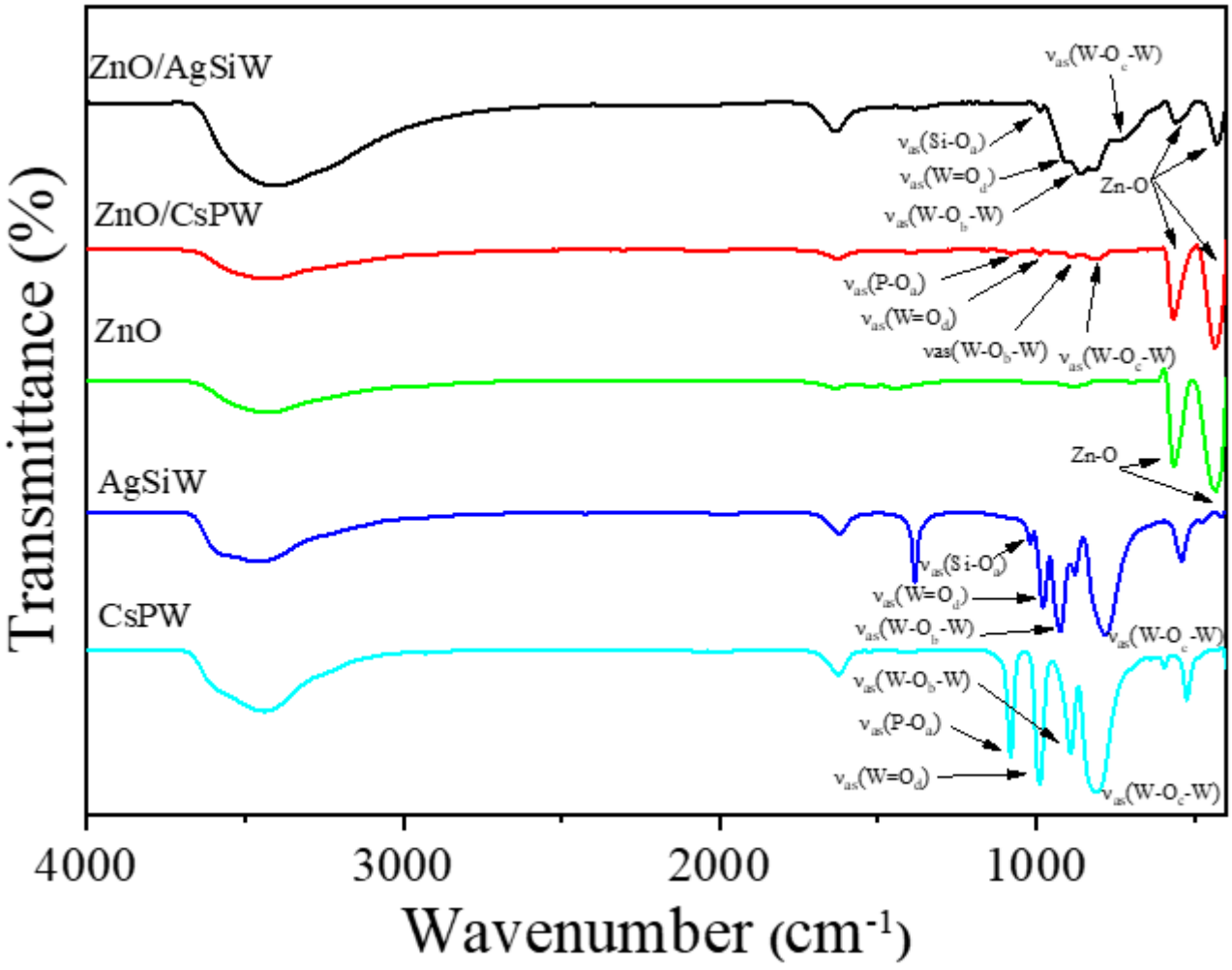

Figure 3

FT-IR spectra of ZnO/AgSiW, ZnO/CsPW, ZnO, AgSiW and CsPW

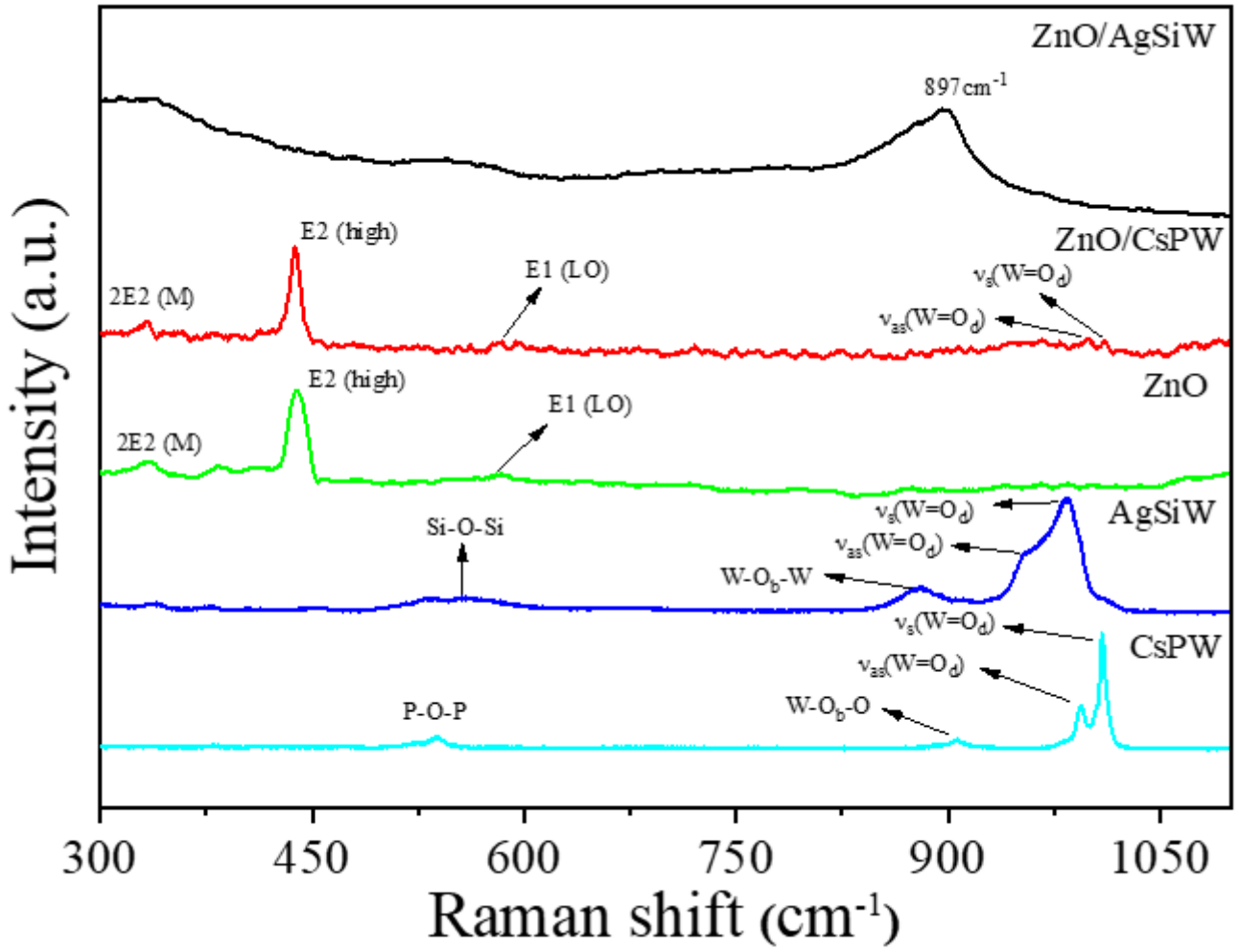

Figure 4

Raman spectra of ZnO/AgSiW, ZnO/CsPW, ZnO, AgSiW and CsPW

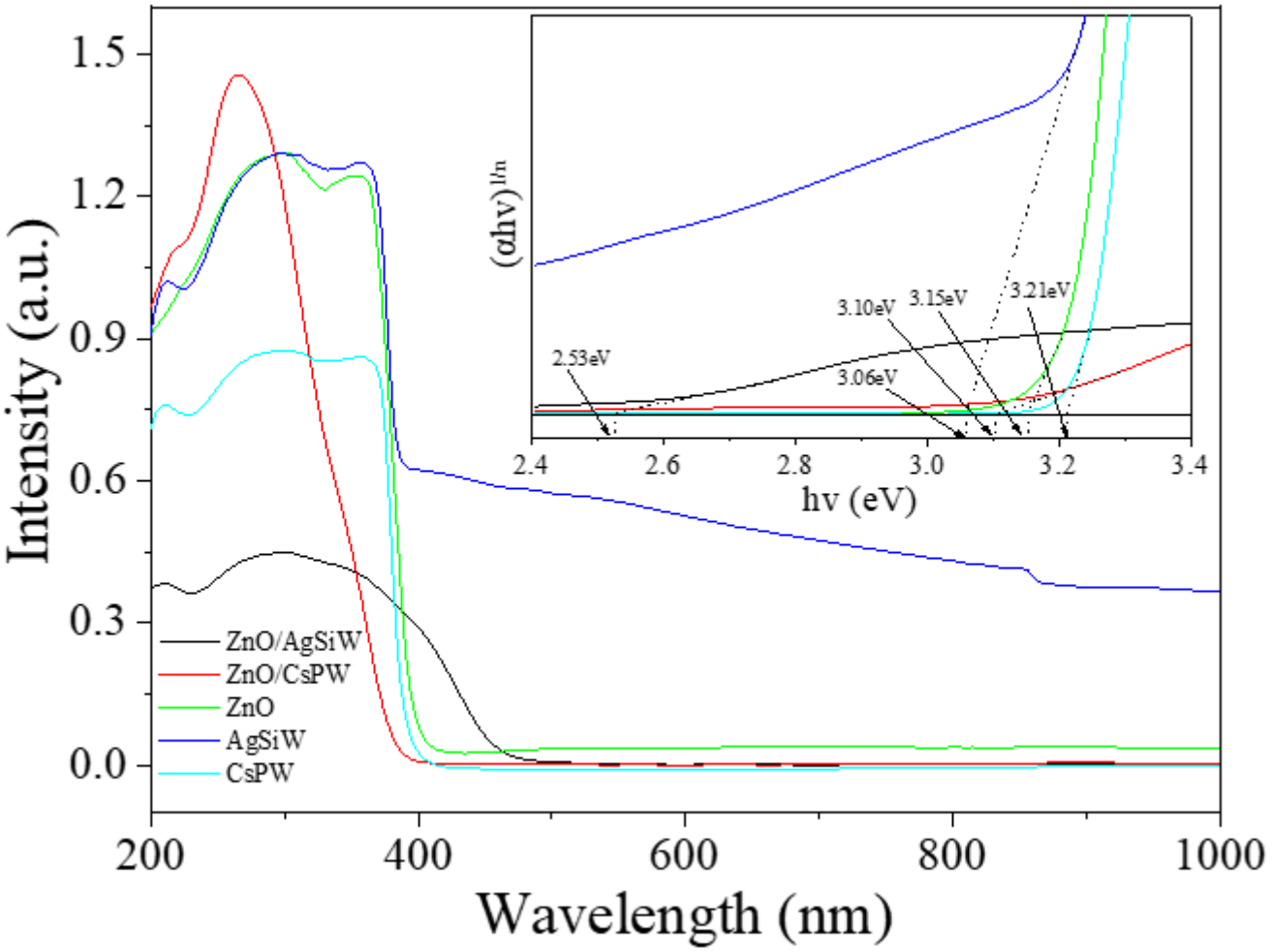

Figure 5

UV-Vis-DRS spectra of ZnO/AgSiW, ZnO/CsPW, ZnO, AgSiW and CsPW

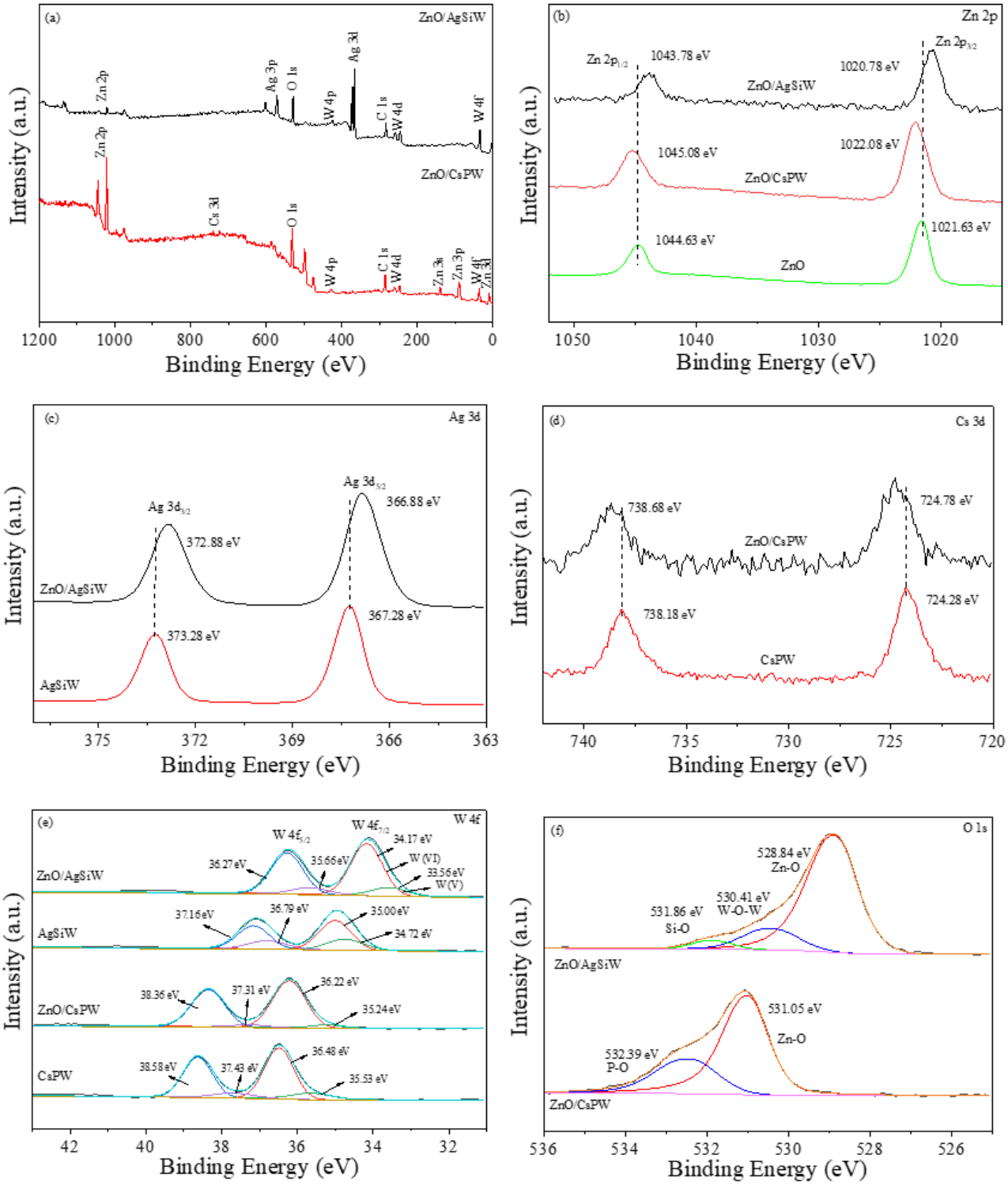

Figure 6

XPS of ZnO/AgSiW and ZnO/CsPW

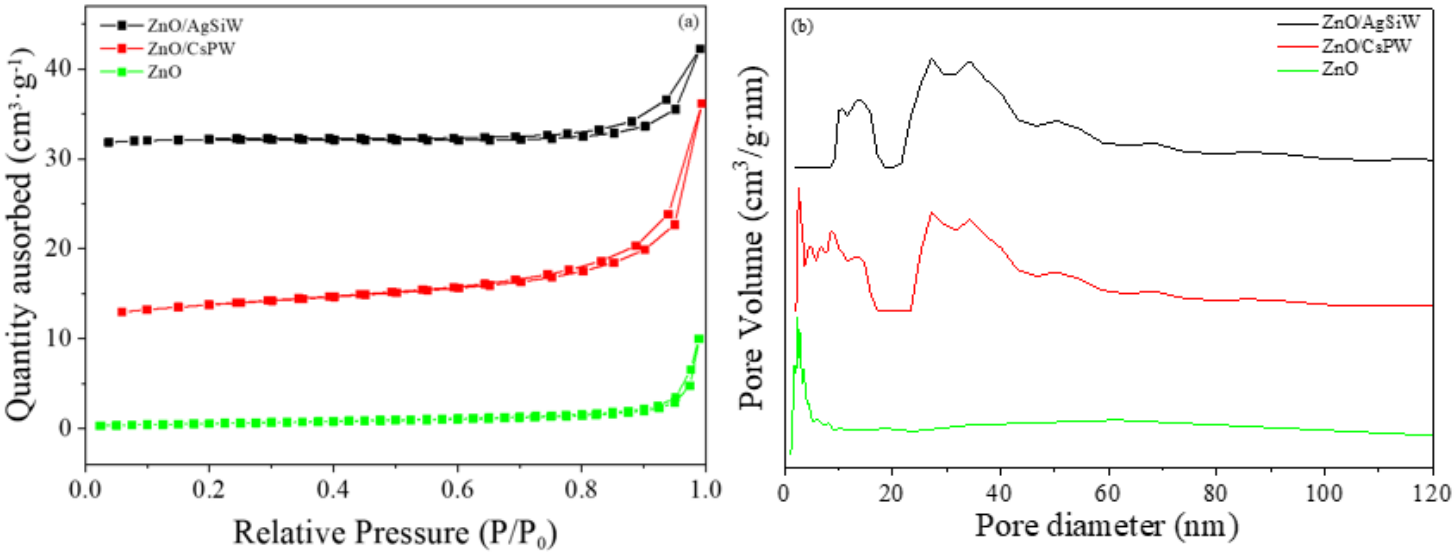

Figure 7

(a) N2 adsorption-desorption isotherms and (b) pore size distribution curves of ZnO/AgSiW, ZnO/CsPW and ZnO

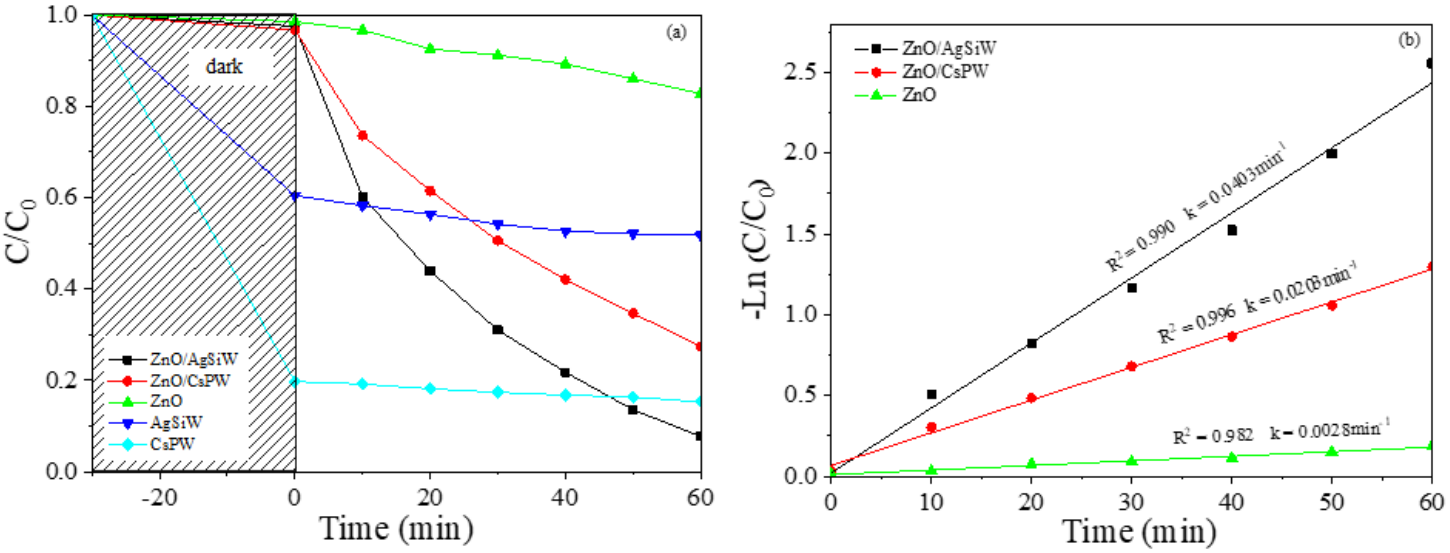

Figure 8

(a) Photocatalytic Rhodamine B degradation; (b) Kinetic constants for RhB degradation using ZnO, ZnO/AgSiW and ZnO/CsPW photocatalysts.

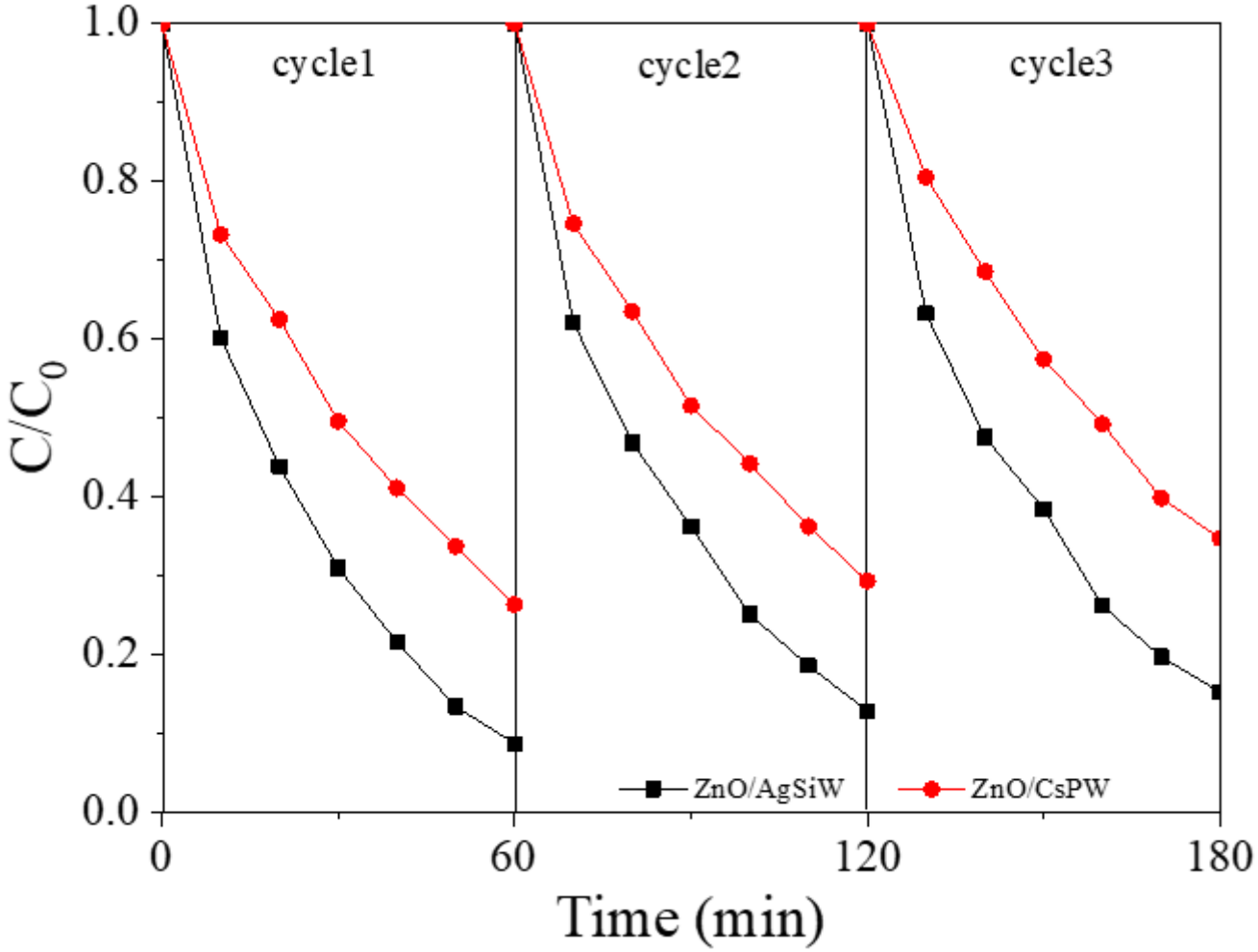

Figure 9

Photocatalytic degradation rate of RhB by recycled ZnO/AgSiW and ZnO/CsPW

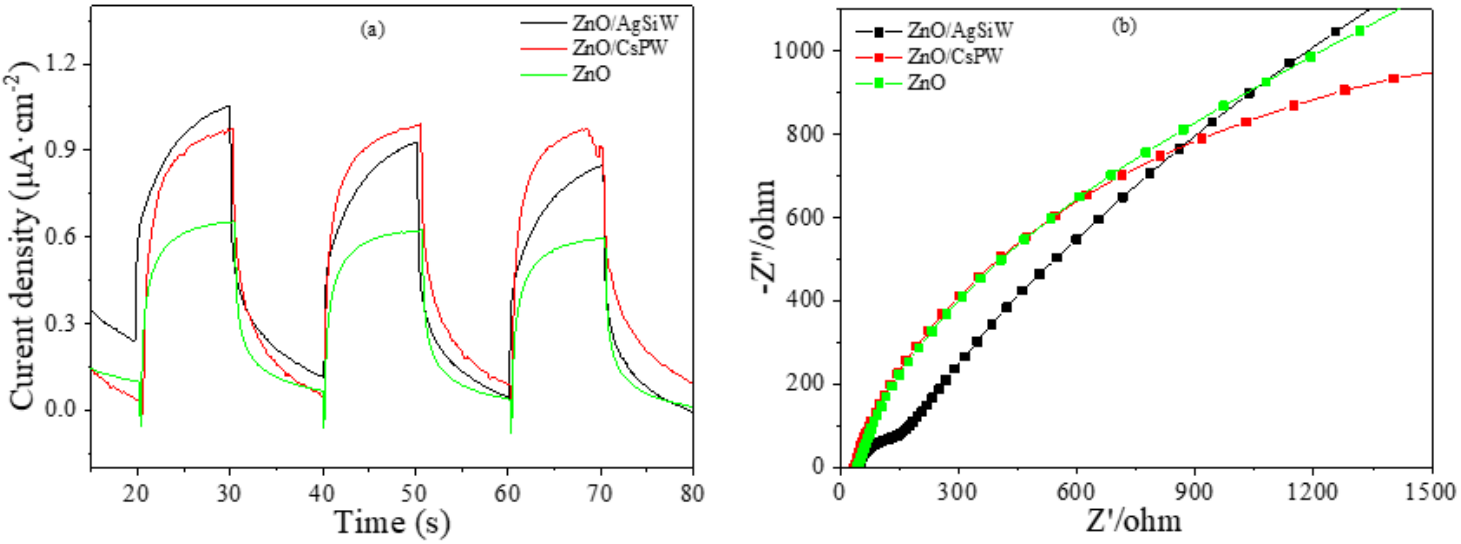

Figure 10

(a) photocurrent response spectra of ZnO, ZnO/AgSiW and ZnO/CsPW, (b) EIS Nyquist plots of ZnO, ZnO/AgSiW and ZnO/CsPW.

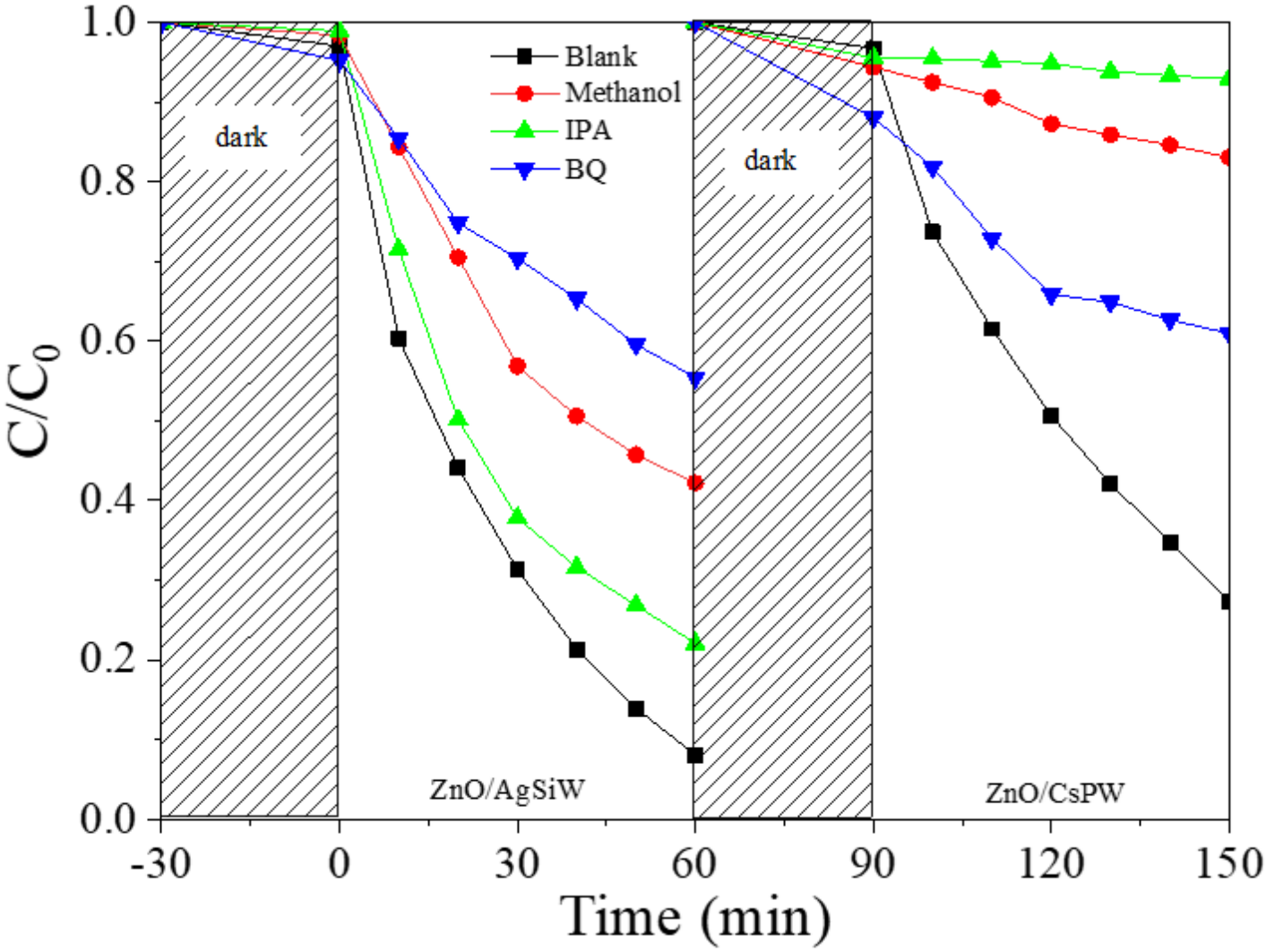

Figure 11

The photocatalytic RhB degradation curve at different free radical scavengers

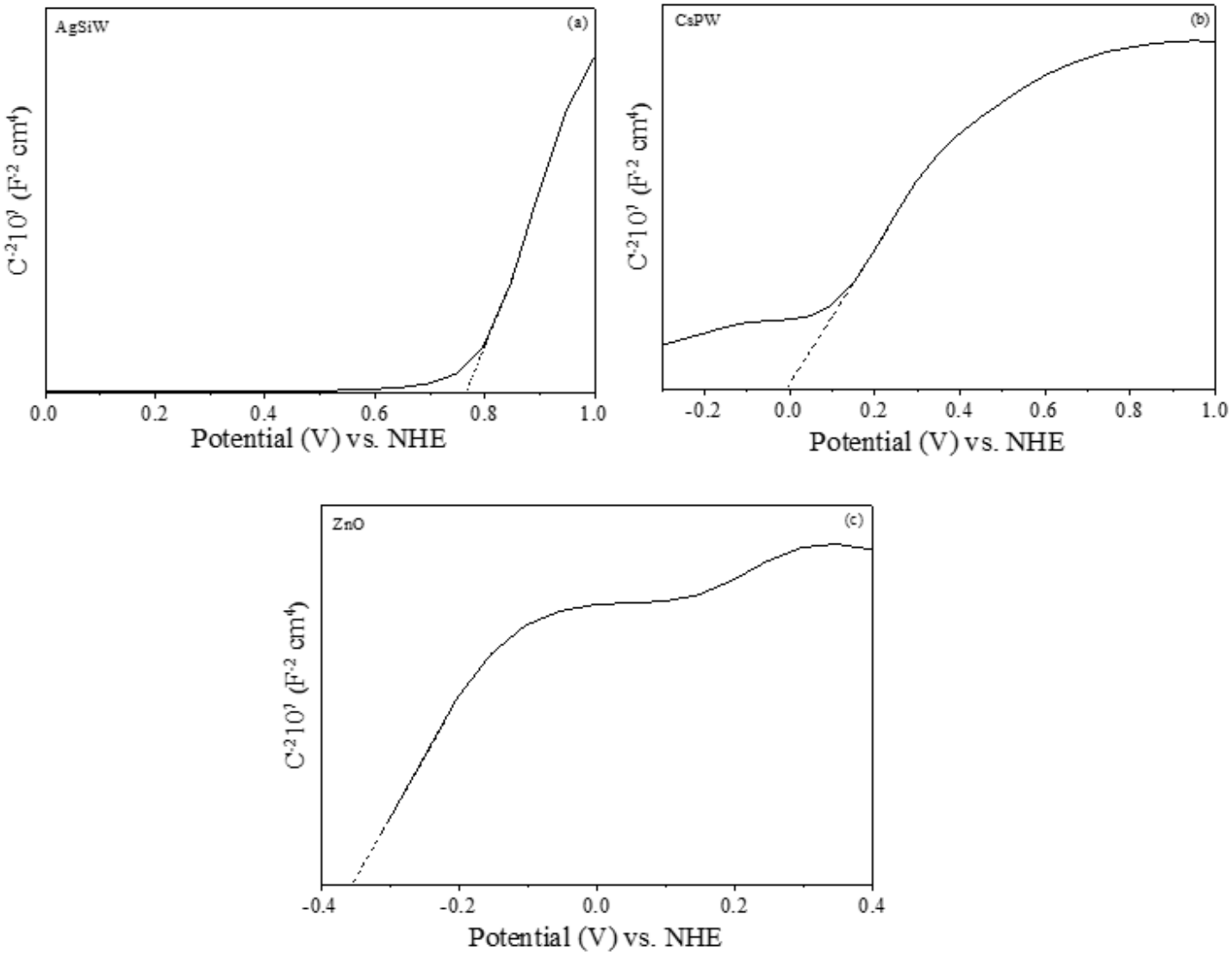

Figure 12

Mott-Schottky plots of ZnO, ZnO/AgSiW and ZnO/CsPW.

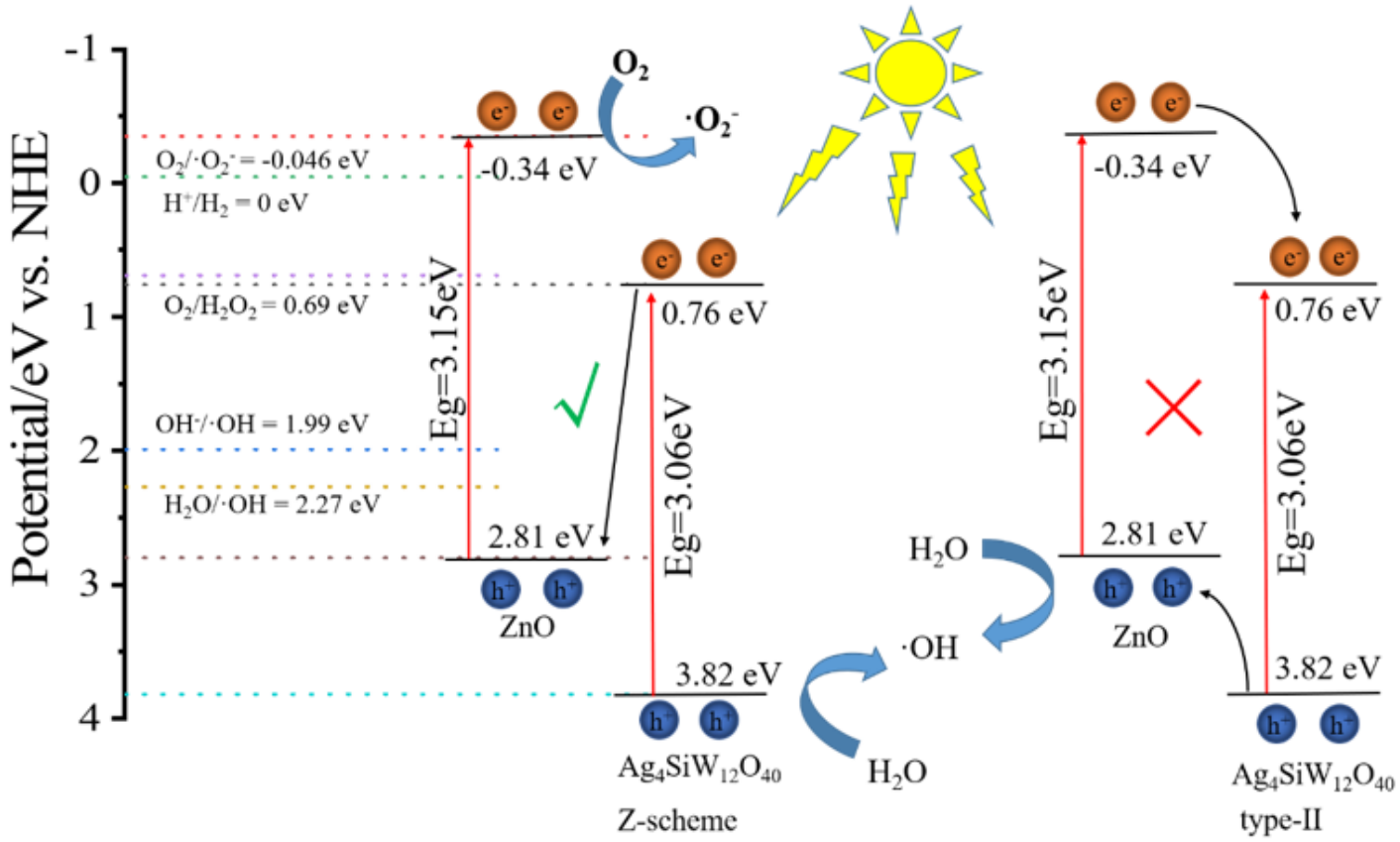

Figure 13

Schematic illustration of photocatalytic activity of ZnO/AgSiW under sunlight irradiation.

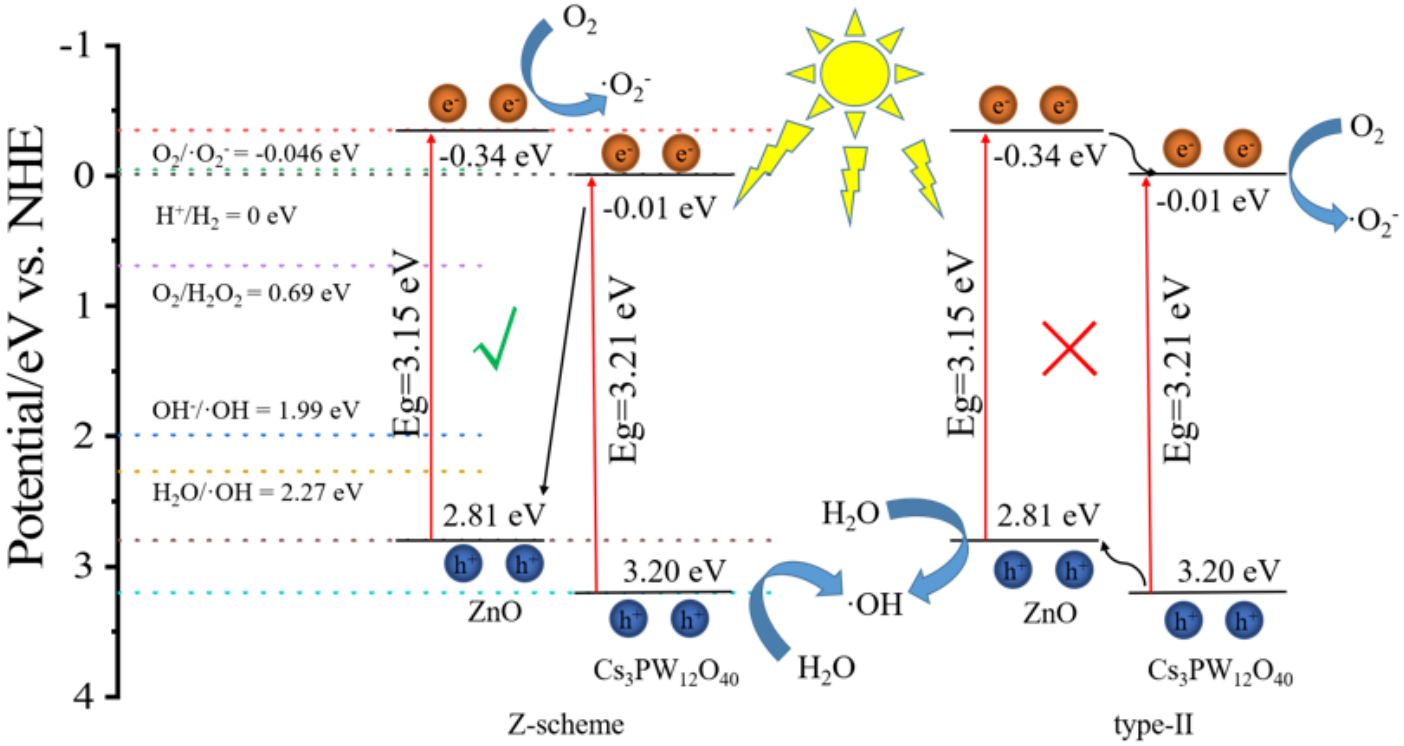

Figure 14

Schematic illustration of photocatalytic activity of ZnO/CsPW under sunlight irradiation.